scientific reports

Check for updates

OPEN

A multi-proxy stalagmite record indicates a shift in forcing of twentieth century drought events in Normandy

Ingrid Bejarano-Arias[1]✉, Carole Nehme[1], Sebastian F. M. Breitenbach[2], Monica Ionita[3,4], James Baldini[5], Edwige Pons-Branchu[6], Sevasti Modestou[2], Stuart Umbo[2] & Damase Mouralis[1]

Drought events are increasingly impacting Europe. The study of past droughts helps disentangle the different factors that trigger hydrological drought, helping to forecast future drought severity. Here we identify the historical drought events of the twentieth and twenty-first centuries in geochemical records of a stalagmite from Caumont cave in Northern France and develop a mechanistic understanding of their root causes. Subannually-resolved stable carbon isotope ($\delta^{13}C$) and trace element data are directly compared with historical climatic records. $\delta^{13}C$, Mg, and Sr peaks align well with most of the historical drought events of the twentieth and twenty-first centuries. The comparison reveals a good correspondence between summer effective rainfall and $\delta^{13}C$, Mg, and Sr concentrations. Further comparison of geochemical records with the precipitation-evapotranspiration index (SPEI) reveals a change in the drought forcings for the past two decades. During most of the twentieth century, droughts appear driven by a pluvial regime, whereas since the late 1990s, drought was driven by higher evapotranspiration due to increased temperature.

Historical records highlight the extended dry phases in north-western France during twentieth century. These dry episodes affected not only Normandy (northern France), but large parts of Western and Central Europe[1,2]. Droughts events are amongst the natural hazards responsible for the most significant economic losses[3], affecting ecosystems[4], agriculture, water and energy supply[5]. Droughts are mainly driven by regional precipitation deficits and/or increased temperature[6,7]. A precipitation deficit is classified as lower than normal conditions in the hydrological system in combination with high (potential) evapotranspiration[5]. Droughts can be classified into four categories, depending on the type of impact: i) meteorological (precipitation deficit over a specific period), ii) agricultural (as a consequence of meteorological conditions that affect crops), iii) hydrological (manifested as reduced river runoff and lake levels after meteorological and agricultural droughts), and iv) socio-economic (negative economic impacts on population)[8].

Given the increasing impact of recent droughts in Europe, resources are being directed towards the reconstruction of past droughts using palaeoclimate archives[9,10]. Tree ring records from the Tatra region, north-western Carpathian mountains, show that during the last millennia, lower temperature align with pandemic episodes across Europe[11]. Additionally, tree rings based reconstructions from the eastern part of Europe indicate that the recent drought events are unmatched over the last 700 years[12].

With global warming as a backdrop, droughts are becoming an increasing concern for modern societies. The recent report from the Group of Intergovernmental Experts about climate evolution[13], confirms a clear trend of increasing European drought, affecting water resources, aquifer recharge, and soil. The droughts of the recent years in France have left many towns with water shortages during the summer[14] and caused the shutdown of nuclear reactors along the Franco-Belgian border[15].

Droughts are well documented in European historical data[16,17], but speleothem records can extend records back further in time, and provide insight where historical records are lacking. Speleothems (secondary

[1]UMR 6266 IDEES, University of Rouen Normandy/CNRS, Mont St-Aignan, France. [2]Department of Geography and Environmental Sciences, Northumbria University, Newcastle upon Tyne, UK. [3]Alfred Wegner Institute Helmholtz Center for Polar and Marine Research, Bremerhaven, Germany. [4]Faculty of Forestry, "Stefan cel Mare, University of Suceava, Suceava, Romania. [5]Department of Earth Sciences, Durham University, Science Labs, South Road, Durham, UK. [6]Laboratoire des Sciences du Climat et de l'Environnement, LSCE/IPSL, CEA-CNRS-UVSQ, Université Paris-Saclay, Gif-sur-Yvette, France. ✉email: ingrid.bejarano-arias@univ-rouen.fr

carbonates deposited in caves) are highly sensitive terrestrial archives that allow the reconstruction of past hydrological conditions at subannual timescales[18–20]. A wide range of environmentally sensitive proxies hosted in stalagmites enable comparisons with contextually robust evidence from historical studies, and the attribution of local environmental changes to regional and pan-regional climatic forcings[21,22].

Here we investigate a recent, well-dated, and highly-resolved stalagmite record from Normandy, north-western France. We investigated the sensitivity of the stalagmite (CCB-1) to drought events and used the stalagmite record combined with historical data to examine the causes of regional twentieth century drought events. Understanding the mechanisms behind drought events will enable assessment of whether the causes have been the same during the twentieth and twenty-first century, or if there has been a change in drought dynamics. We combined stable carbon isotope ratios ($\delta^{13}C$) with trace elements (Mg, Sr) to reconstruct changes in local hydrology. We used the Mg and Sr records as recorders of prior carbonate precipitation (PCP) which is enhanced during drier periods[23–25]. We then compared these data with historical and meteorological records (temperature, effective infiltration) and the twentieth century standardized potential evapotranspiration index (SPEI)[26]. This combination of data allows for differentiation of the mechanisms of drought, whether by pluvial or temperature regime.

Normandy, northern France (Fig. 1a) rests largely on a chalk plateau incised by the Seine River. This incision has resulted in long-term groundwater table lowering along a 120 m deep valley, facilitating vadose cave system formation[27] such as our study site, the Caumont quarry and cave system (CQCS) (Fig. 1b). The CQCS is located ca. 25 km southwest of Rouen (N 49°22′41″; E 0°54′47″; 15 m above sea level)[28,29] (Fig. 1c), with ~ 115 m of limestone overburden[30]. Exploited for building stone since the Middle Ages, CQCS today reaches a total length of ca. 13 km, accessible via the main entrance, located ca. 200 m from the Seine River[31] (Fig. 1c). Inscriptions on the gallery ceiling at the sampling site, indicate opening and excavation dates, providing direct age information (Fig. 1b).

The climate of Normandy is temperate oceanic[32], with the dry season between April and September

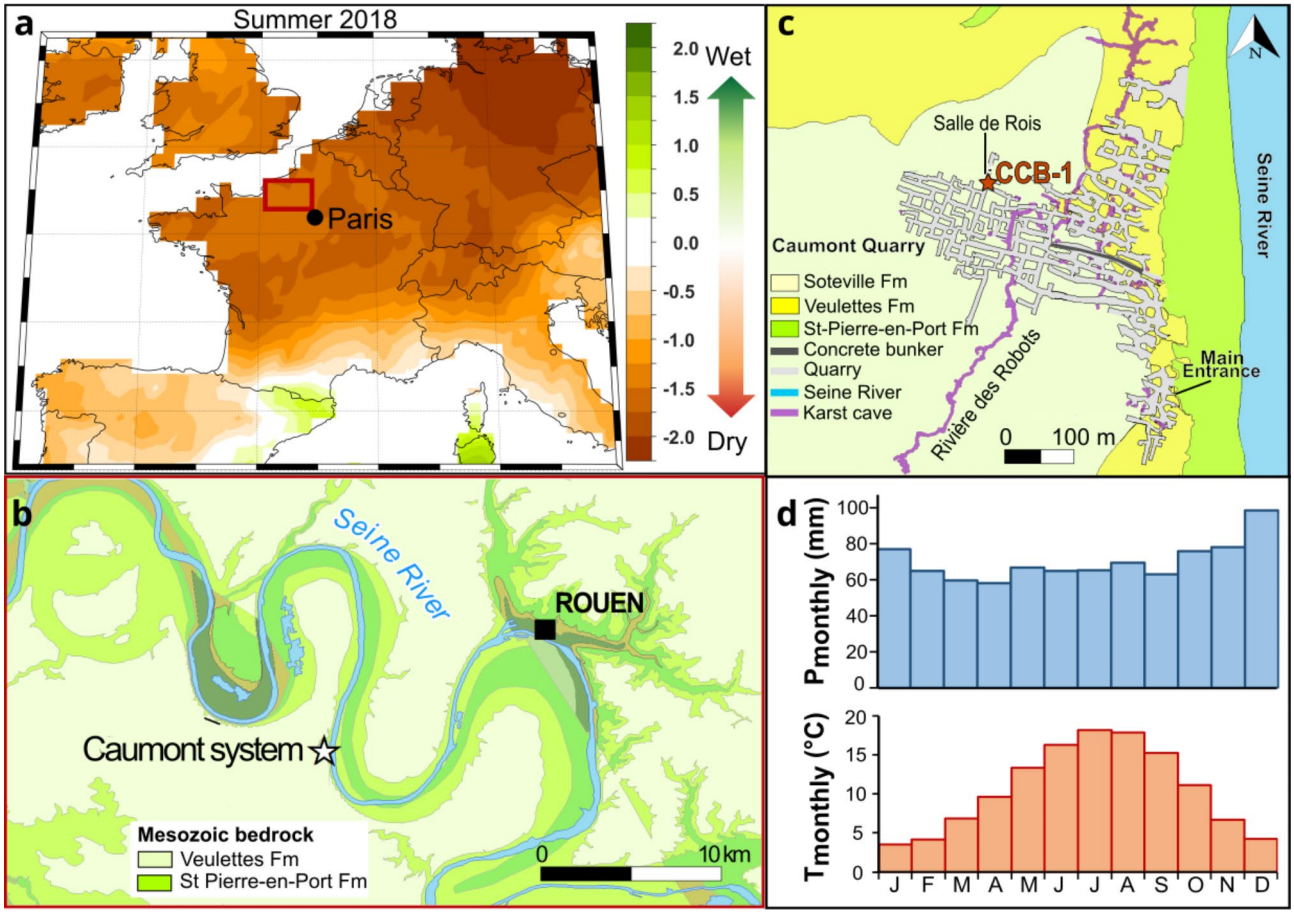

Fig. 1. Location map of the study area. Map of western Europe of October SPEI6 displaying drought conditions during summer 2018, and the location of the Seine River (red rectangle). Map generated with Matlab version 2024a (**a**). Location of the CQCS (white star) (**b**), and the sampling site of the stalagmite CCB-1 (red star (**c**)), in Salle des Rois located 800 m from the quarry entrance. Maps modified from Ballesteros et al.[32], generated with ArcMap version 10.8. Monthly values of precipitation and temperature in Rouen meteorological station from 1990–2018 (**d**).

and the wettest from October to January[33]. Here, the dry season corresponds to the summer season, when evapotranspiration is higher and infiltration is reduced. The closest meteorological station, Rouen-Boos, located 20 km from CQCS, records total annual rainfall between 418 and 1065 mm[33]. Effective infiltration describes the precipitation amount infiltrating the soil, layers above the cave, and entering the cave[19]. In Caumont, the highest effective infiltration is during autumn and winter[28]. Surface air temperatures range from 4 °C to 18 °C, with July and August being the warmest months, and January the coldest (Fig. 1d). Potential evapotranspiration (PET) is highest in spring and summer[34], resulting in minimal effective infiltration into the epikarst above the cave during the summer season. Cave air temperature at the sampling site is very stable (10–11 °C) and very close to the mean annual air temperature (10.6 °C)[28].

Results

Dating and age model for stalagmite CCB-1

The chronology of stalagmite CCB-1 (4 cm in length) is based on U-series dating and constrained by historical information. Three U-series dates suggest continuous growth since ~ 1907 (Figure S1, Table S1). Age correction was applied to the detrital ^{230}Th based on stratigraphic constraints using the STRUT ages routine[35]. Due to the moderate U concentration of 0.2 to 0.4 ppm and relatively low Th content (0.3 to 8.9 ppb), corrected ages (Table S1) include uncertainty of ± 40 to ± 60 years. To further improve the chronology, we counted individual laminae through greyscale analysis, assuming that these represent seasonal changes in carbonate deposition. This layer counting chronology was linked to calendar age by assigning the top of the stalagmite to 2019 CE (the year of sampling) as maximum age. The final age model was constructed using the layer counting information and the COPRA routine[36].

The age-depth model reveals that the stalagmite grew over the period of 1914 to 2018 CE. The layer counting age model agrees well with the U-series growth estimate, but is internally more precise because most individual layers are easily identified in the grey scale record. The layer counting model is also consistent with an inscription (1901 CE) on the ceiling of the sampling chamber that indicates the year when this gallery was excavated. Thus, the stalagmite growth is constrained by the two ages of 1901 and 2019 CE (Figure S2). The fact that carbonate deposition began a few years after the chamber was opened is likely explained by ongoing quarrying works that disturbed the floor in this chamber and hindered speleothem deposition between 1901 and 1914 CE. This effect has been previously observed at Brown's Folly mine, UK; where stalagmite growth lagged after closure of the mine combined with a delay in soil recuperation[37]. Stalagmite CCB-1's growth rate was relatively high, 0.40 mm/a, with the highest growth rate occurring from 1926–1927 and 1944–1945 CE (0.74 mm/a). The lowest in 1940 CE (0.12 mm/a). The fact that stalagmite CCB-1 is modern permits comparison of the stalagmite's records with instrumental data of the twentieth and twenty-first century.

Instrumental records and drought events in the twentieth and twenty-first century

Normandy receives ca. 750 mm of precipitation annually. The first half of the twentieth century was generally drier; the lowest annual precipitation totals were 418 mm in 1921 and 431 mm in 1953 (Fig. 2). The highest precipitation on record fell in 1999, 2000, and 2001, with annual totals of 1041, 1065 and 1057 mm respectively. After 1977, rainfall at the site increased from 804 mm/yr to 1065 mm/yr in 2000, with a below average decrease in precipitation of 524 mm/yr in 1989 (Fig. 2b). Effective infiltration is estimated by subtracting evapotranspiration from total precipitation[38]. The lowest effective infiltration in Normandy is estimated to have occurred in 1921 (167 mm) and the highest in 1910 with 857 mm (Fig. 3d).

The mean annual temperature (MAT) over the instrumental record is 10.6 °C, with a maximum MAT of 12 °C (1949) and a minimum of 9.1 °C (1963, 1985 and 1987) (Fig. 2). From 1921 until 1961, MAT were higher (averaging 10.9 °C), then reducing to 10.6 °C between 1962 and1995. From 1996 onwards, there is a clear trend towards higher temperatures (Fig. 2c), with consistently warmer MAT (reaching 11.9 °C during 2014 and 2018).

The most significant twentieth and twenty-first centuries (meteorological) drought events in France occurred in 1921, 1934, the 1940s, 1976, 1989, 2003 and 2018 (Fig. 3g, Table S2)[1,39–44]. These droughts have been described as severe calamities that impacted economies and agriculture in France and elsewhere[45–48]. Drought events affect hydrology and water resources, which directly impact agriculture by reducing crop yields and production, thereby the economy[49,50]. The most extreme drought of the 20th Century occurred between 1920 and 1922[40,44]. During this event, a minimum discharge of 20 $m^3 s^{-1}$ was recorded in the Seine River[51]. During the 2003 drought, French maize and wheat fields experienced historical lows in production[52].

Stable isotope and trace element composition of CCB-1

In this study, we focused mainly on the $\delta^{13}C$ record; the $\delta^{18}O$ record is described in the supplementary results. The $\delta^{13}C$ record displays significant variations, with a maximum of -7.8 ‰ and minimum of -12 ‰. Distinct higher excursions, occur at ca. 1921 and 1936, and double peaks of higher values around 1948–1953, 1973–1976, and 1995–2001 CE (Fig. 3a). These years are close to several low rainfall periods noted above (Fig. 2). Since ~ 2003 CE, the $\delta^{13}C$ profile shows a trend to higher values.

The magnesium (Mg) and strontium (Sr) records are positively correlated with $\delta^{13}C$ ($r = 0.66$ and 0.58, respectively), with distinctive peaks during the early 1920s, and 1930s, late 1940s and 1950s and 1973–1976 CE. Mg exhibits the highest correlation with $\delta^{13}C$ and ranges between 58.3–950.8 ppm (Fig. 3b), Sr ranges between 3.6–80.6 ppm (Fig. 3c).

Previous studies have shown that the stable isotope and elemental records are highly influenced by infiltration processes in the epikarst. Cave monitoring at the CQCS site has shown that seasonal precipitation amount controls infiltration and that $\delta^{13}C$, Mg, and Sr speleothem records are generally driven by infiltration dynamics during the summer months[28]. During the summer both evapotranspiration and a longer water residence time in the epikarst enhance PCP and increase isotope ratios[53–55]. We use $\delta^{13}C$, Mg and Sr as hydrological indicators

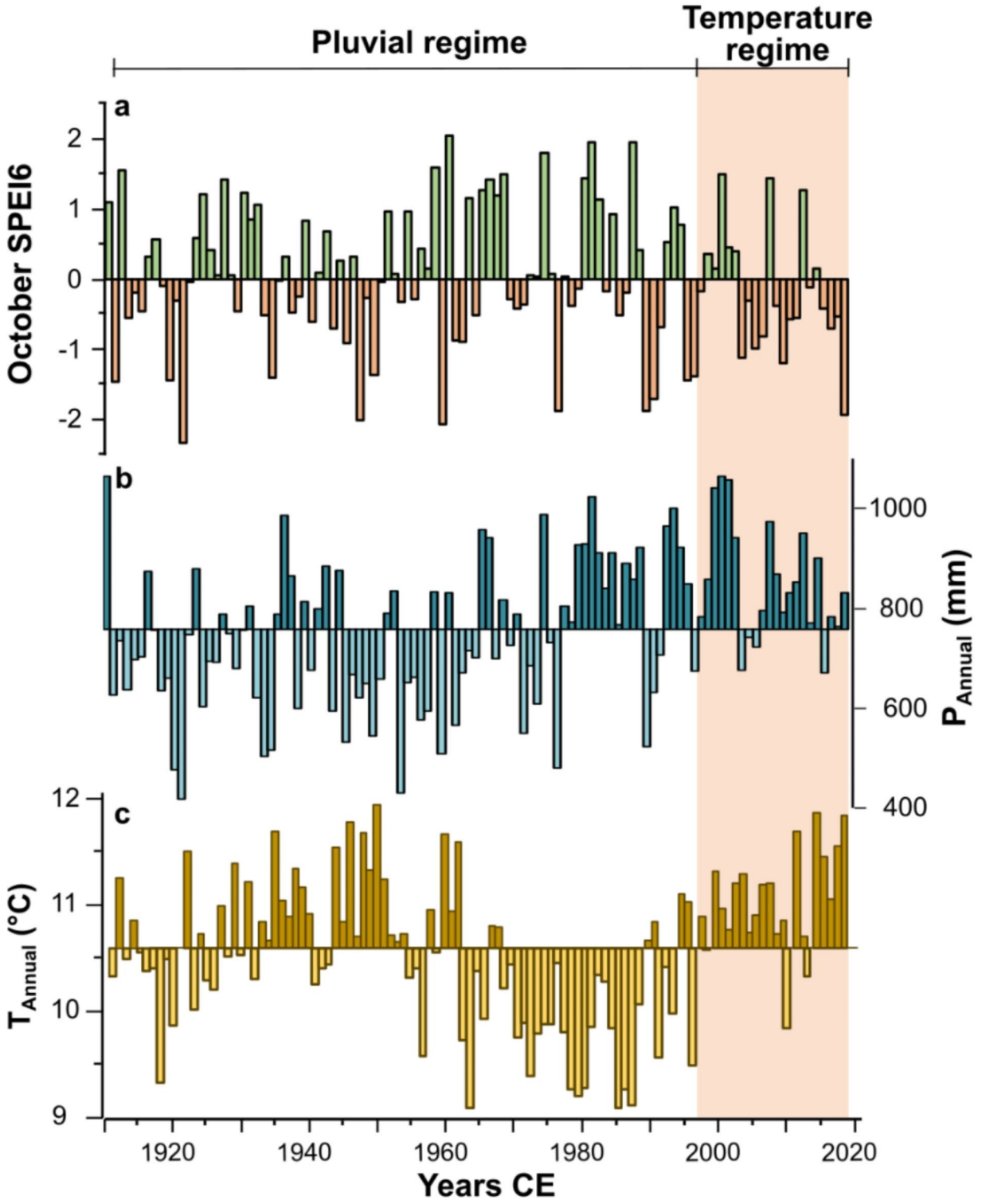

Fig. 2. Since the late 1990s (orange shading), Normandy remains water stressed (**a**), despite above average rainfall (**b**); likely due to increased air temperature (**c**) which enhance evapotranspiration. Dry events (negative SPEI values) are mostly correlated to higher temperatures (and thus higher evapotranspiration; 'Temperature regime'), compared to previous periods where negative SPEI appears correlated to decreased precipitation ('Pluvial regime').

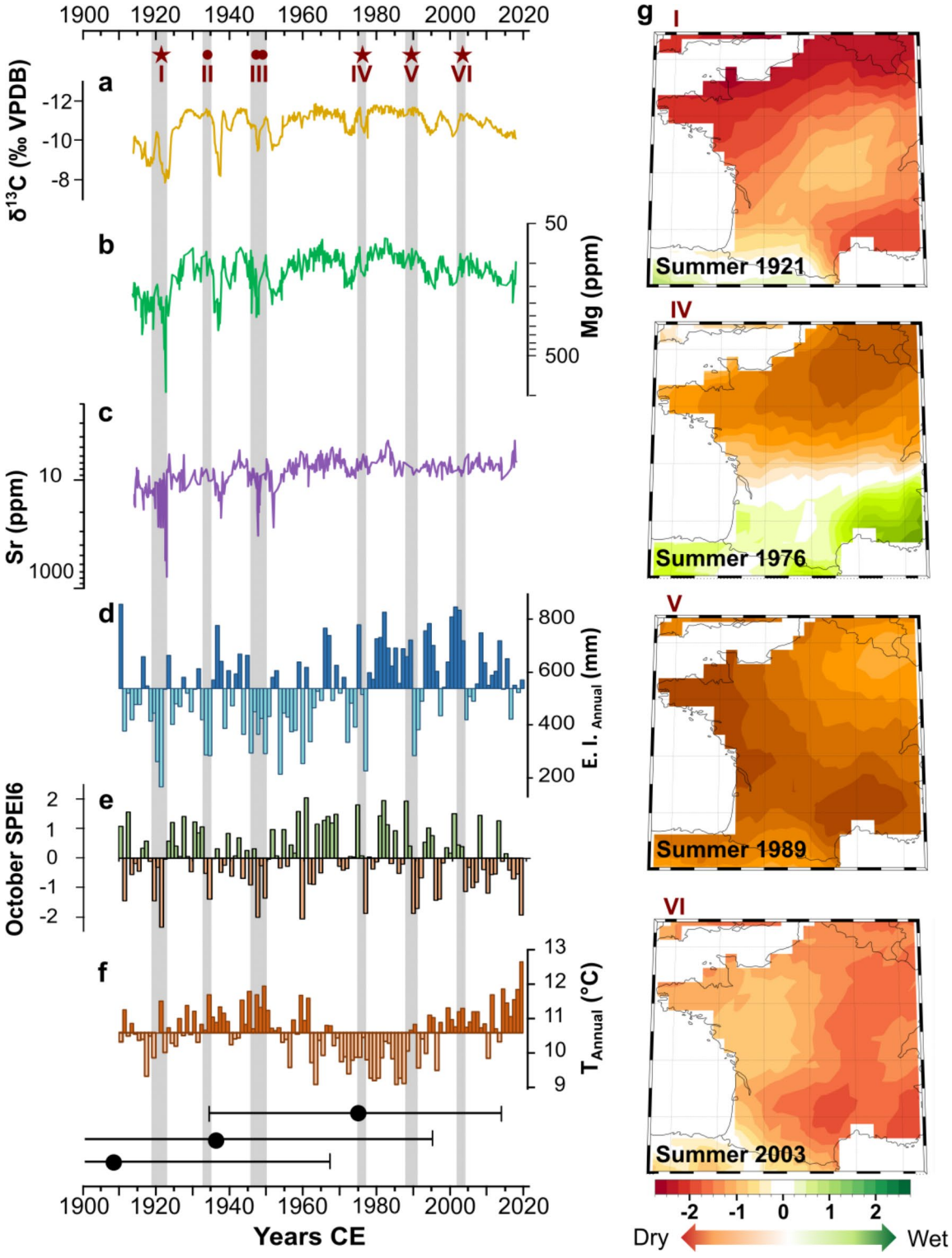

Fig. 3. Speleothem multi-proxy record reflects local hydroclimate. Geochemical time series include $\delta^{13}C$ (**a**), Mg (ppm) (**b**) and Sr (ppm) (**c**). Note that the y-axis is inverted. Climate time series: effective infiltration (**d**), October SPEI6 (**e**) and annual temperature of the twentieth century (**f**). Black dots are U/Th ages (1907 ± 60, 1935 ± 40, 1974 ± 40). Grey shades represent historical droughts with the dark red dots corresponding to local scale and dark red stars correspond to regional scale. Maps of October SPEI6 that correspond to the intensity of the dry conditions, centred over France, during the years 1921, 1976, 1989 and 2003, which represent four of the historical droughts of the twentieth and twenty-first centuries. Maps generated with Matlab version 2024a (**g**).

with higher values reflecting drier conditions above the CQCS site. We find the covariability between the proxy records of CCB-1 with the instrumental data convincing (Fig. 3).

Links between the drought index and the stalagmite proxy record

For the current study we tested different accumulation periods for SPEI (e.g., 6-months and 12 months). We used the accumulation period of 6 months for October, corresponding from May to October and covering the summer months. October SPEI6 presented the highest correlation with our record (Fig. 2a) (see methods section for more details). Consequently, to identify the summer dry events of the twentieth century, we use the October SPEI6 record. This record ranges from -2.34 in 1921 (extreme dry) to 2.05 in 1960 (extreme wet). Between 1919 and 1959, the October SPEI6 record also shows several multi-annual phases of below-average infiltration (e.g., 1919–20, 1933–34, 1937–38, 1947–49) (Fig. 2a). Between 1959 and ~ 1985, the October SPEI6 record indicates overall wetter conditions, except for 1976 which recorded well below average infiltration (-1.87). Since the 1990s, October SPEI6 indicates regional conditions became increasingly drier, with an increasing frequency of dry events and very few positive infiltration years (e.g., 2018).

October SPEI6 dry events align with $\delta^{13}C$ peaks during severe (-1.5 to -2) and extreme dry conditions (< -2) (Fig. 3). This is most apparent for the years 1921, 1947, 1976 and 1995 CE (Table S2). Likewise, the peaks of higher Mg and Sr values are identified for years 1921, 1937 and 1946–47. The positive trend of $\delta^{13}C$ since 2003 agrees with a higher frequency of dry years, reflected in the October SPEI6 timeseries. In the last two decades, relatively dry conditions occurred almost every year, except for years 2007 and 2013 (Fig. 3e).

Discussion

Precipitation and potential evapotranspiration are used as the indicators for SPEI[50], which allows us to use this index as a regional record of effective moisture budget, with elevated SPEI indicating wetter conditions. The total annual rainfall has increased since the 1970s, reducing the number of years with negative rainfall anomalies (Fig. 2b). A closer look into the temperature record shows continuously warmer conditions since the late 1990s, which is supported by a higher frequency of negative October SPEI6 values in this region since 1989 (Fig. 2a). This appears at odds with the increase in total precipitation in the region (Fig. 2b), but we propose the discrepancy between increasing rainfall totals and infiltration deficit, reflected in the October SPEI6 timeseries (Fig. 3e), could be explained by the rise in temperature since the 1990s (Fig. 3f).

Below, we evaluate how these hydrological changes are recorded in stalagmite CCB-1 over the twentieth century. Lower effective infiltration increases PCP, which then increases $\delta^{13}C$ and Mg concentration in the stalagmite[38,56]. Since effective precipitation is lowest during the summer months when evapotranspiration is highest, the PCP signal is biased towards the warm season[28]. We find a very good correspondence between the PCP indicators ($\delta^{13}C$, Mg and Sr) and effective precipitation, with higher ratios correlating to periods of effective infiltration deficit (Fig. 3d). Our reconstruction reveals a striking pattern of infiltration minima double peaks (Fig. 3a), which can be directly related to infiltration minima (e.g.: 1920–21, 1932–34, 1945–50, 1953–57, 1971–73, 1989–91) as seen in the October SPEI6 record, especially in the first half of the twentieth century, e.g., in 1921 CE (Fig. 3e). The link between years of deficient effective infiltration and higher $\delta^{13}C$ and Mg values in ca. 1934–1937 CE and both the 1940s and 1950s is less obvious but still discernible. In the second half of the twentieth century, PCP periods are detected in the intervals 1972–1976 and 1994–2003 CE.

The correspondence of $\delta^{13}C$ and Mg maxima with minimal effective infiltration seems less evident during the second half of the twentieth century, although $\delta^{13}C$ record still displays a trend towards higher values from ca. 2003 that suggest declining infiltration (Fig. 3). It is possible that crossing a certain infiltration threshold is needed to initiate PCP-associated Mg and Sr shifts.

The CCB-1 multi-proxy record ($\delta^{13}C$, Mg, and Sr) shows distinct and repeated positive excursions for the years 1921, the late 1930s, the late 1940s, the late 1970s, and 2003 that reflect a lack of infiltration (Fig. 3). These one-to-four year long excursions can be linked to: i) reduced effective infiltration in the epikarst above the cave, ii) enhanced PCP in the epikarst and cave, and iii) lower drip rates and enhanced CO_2 degassing[25,28,54,57,58]. The fact that the Mg, Sr, and $\delta^{13}C$ records all show similar dynamics support our interpretation that PCP is a key influencing parameter which itself is driven by local hydroclimatic conditions above the cave. The clear relation between the isotopic and trace element records and the October SPEI6 timeseries strongly support the fidelity of the stalagmite archive to record seasonal to multiannual climate conditions, and especially droughts. Consequently, the agreement between stalagmite-based geochemical records, instrumental data, and the October SPEI6 help to recognise historical drought events of the last ca. 120 years, including 1921, late 1940s, 1976, and 2003. The faithful record of climate variations of the twentieth and twenty-first centuries in CCB-1, indicates that we could confidently extend the record further back in time in the CQCS.

Droughts are complex climatic events which are driven by precipitation deficit or temperature[17,47,59]. The comparison with the instrumental temperature records shows that the years of high values correspond with heavier $\delta^{13}C$ signal peaks for the years 1921, late 1930s, late 1940s and late 1990s (Fig. 3a). The first peaks from the Mg and Sr records are also in agreement with warmer years of 1921, late 1930s, late 1940s and 1950s (Fig. 3b,c). This provides further evidence that high temperatures during the summer months enhance evapotranspiration which consequently influences the isotopic signal in the epikarst and leads to higher PCP. Figure 3 highlights the correspondence between increasing $\delta^{13}C$ ratios, high Mg and Sr values, low effective infiltration, severe and extreme dry events according to the October SPEI6 index, and higher temperatures. These parameters align well with the historical droughts of the years 1921, the end of 1940s and 1976 CE, suggesting that the drought events for the first part of the twentieth century are related to a precipitation deficit, (pluvial regime). However, the correspondence is less evident for both years 1989 and 2003 CE.

From the year 1996 onwards, we observe an increasing temperature trend (Fig. 2b), with higher MATs (reaching 11.9 °C during 2014 and 2018). This trend aligns well with the trend of higher $\delta^{13}C$ values (Fig. 3) since

the early 2000s onwards. Constant warmer conditions since the late 1990s could explain the trend of elevated $\delta^{13}C$ record, even if precipitation records for the last two decades show no major precipitation reduction (Fig. 2b). This relationship reinforces that higher surface temperature since that time has a more significant influence on the stable isotope signal (temperature regime) than precipitation deficit[48]. Other studies have also shown the shift in drought regime over the last 120 years, where surface temperature and potential evapotranspiration in soils have a significant effect on drought dynamics in Europe[60]. Vicente-Serrano et al.[26] suggested increasing drying trends from global SPEI datasets, partially due to increasing temperature from the mid-1980s[61].

Further analysis of isotopic records shows that among the higher values classified as drought, we identified a variation in the isotopic signal separating the points in two clusters, of higher (orange dots) and lighter isotopes (yellow dots) (Fig. 4a). This difference between the drought clusters is more evident within the $\delta^{13}C$ record, with a 1.28 ‰ difference (between heavier and lighter), than for $\delta^{18}O$ (0.18 ‰) (Fig. 4b). Comparing the drought clusters to the temperature record, it is apparent that years with the lighter signal (yellow dots), match with the increasing trend in the temperature record after 2000s (Figure S3). Increasing temperatures usually enhance soil respiration, producing a lighter $\delta^{13}C$ signal[19,54], which is in accordance with a lighter drought $\delta^{13}C$ values compared to the heavier drought cluster at the beginning of the twentieth century. However, the average of the lighter $\delta^{13}C$ cluster (-10.31‰), still shows a heavier signal than the rest of the record (mean = -10.75 ‰). This reflects the impact that increasing temperature has at the surface over recent decades, by enhancing evapotranspiration even though there is no deficit in precipitation. The lighter isotopic drought cluster reflects then the change in drought dynamics from a pluvial regime to a more temperature and evapotranspiration related process.

A study based on SPEI and other drought indexes in Europe for the last 104 years (e.g., Standardized precipitation index – SPI; Palmer drought severity index – PDSI) also identified an increase in severe and extreme droughts since ca.1990[60,62]. The central and southern parts of Europe are becoming dryer as a result of increasing PET and mean air temperature[60]. This drying trend in soil and in the epikarst is confirmed in Normandy, through the convergence of the geochemical proxies evidenced in the stalagmite CCB-1, with the SPEI index and historical data. Our results show that the climatic conditions of the past century recorded within the CQCS are consistent with the regional palaeoclimate dynamics of north-western Europe.

Analysis of the different drought events recorded in CQCS shows the complexity of drought events, their irregularity and how different climatic parameters (i.e., precipitation and temperature), can change over time. We show that using these proxies together ($\delta^{13}C$, Mg and Sr) is critical to disentangle the complex mechanisms underlying drought events. In the case of CC1-B, this combination made it possible to differentiate the impact of effective infiltration versus temperature changes. Additionally, to identify the shift in drought dynamics, transitioning from primarily precipitation-controlled events in the twentieth century to a regime increasingly dominated by rising temperatures in recent decades. Our results align with observed trends of more frequent droughts and future climate projections, emphasizing the escalating influence of rising temperatures due to climate change on European drought patterns and the urgent need for adaptive water management strategies.

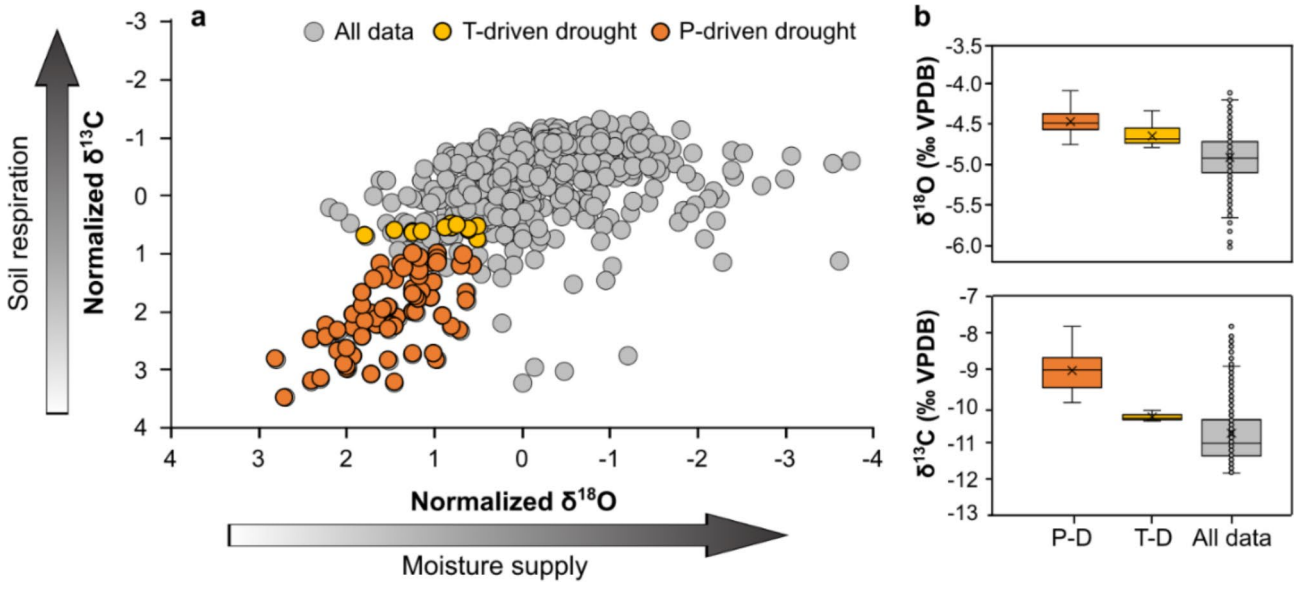

Fig. 4. Precipitation-driven droughts can be differentiated in $\delta^{13}C$ – $\delta^{18}O$ space. $\delta^{13}C$ vs $\delta^{18}O$ relationship in stalagmite CCB-1 (**a**) (Isotope values are z-score normalised). Drought years are identified as positive values, which can be further subdivided in two clusters corresponding to i) pluvial (P-D) and ii) temperature (T-D) drought regimes. Arrows indicate the direction of the main forcings (soil respiration and moisture supply). Box plots for $\delta^{18}O$ and $\delta^{13}C$ signals depict the signal difference between the two drought clusters (**b**).

Methods

Stalagmite CCB-1 and sample preparation

The stalagmite CCB-1 was collected in 2019 from the "Salle des Rois", a quarry chamber of the CQCS. At the time of collection, the stalagmite was still actively growing and the Salle des Rois had current drip. CCB-1, composed of calcite, was cut in four parallel slabs, from which the centre slab (110 mm wide and 38.6 mm long) was placed in epoxy resin, polished to improve appearance of growth laminae and other structures, and subsampled. Polishing was performed with silicon carbide sandpaper, from 120 to 2400 µm. Subsampling was performed for geochronological (U-Th) and geochemical ($\delta^{18}O$, $\delta^{13}C$, trace element) analysis.

U/Th dating

Three powder samples were taken for U-Th dating at 1, 22, and 34 mm from top of the stalagmite CCB-1 using a 1 mm drill bit (Figure S1). Powder samples of 90 to 150 mg were dissolved in PTFE beakers and mixed with a ^{229}Th-^{236}U spike. This spike solution was calibrated against HU-1 uraninite, assumed to be at secular equilibrium. After co-precipitation with $Fe(OH)_3$, the uranium (U) and thorium (Th) fractions were separated and purified using U-TEVA® in nitric media (HNO_3 3N), with Th and U elution in hydrochloric acid (3N and 1N HCl, respectively). The U and Th isotopic composition was analysed at the Laboratoire des Sciences du Climat et de l'Environnement (LSCE, France), on a Multi-Collector Inductively Coupled Plasma Mass Spectrometer (MC-ICPMS) Thermo Scientific™ NeptunePlus fitted with an Aridus II™ introduction system and a jet pump interface. The detailed chemical treatment and MC-ICPMS analysis are outlined in[63,64]. After corrections for mass fractionation (using an exponential law), peak tailing, hydrate interference, and chemical blanks, $^{230}Th/^{234}U$ raw ages were calculated through iterative age estimation using the ^{230}Th, ^{234}U and ^{238}U decay constants of Cheng et al . (2013)[65] and Jaffey et al.[66].

Laminae counting and greyscale analysis

The stalagmite exhibits growth layers that are visible to the naked eye (Figure S4). The growth layers have been identified by grey value changes, with dense translucent layers being deposited in one season, and more milky-white layers being formed in another season. Although it currently remains impossible to unambiguously ascertain when exactly each layer is formed, we counted greyscale value maxima to develop a layer counting chronology following the method outlined in[67]. To extract greyscale data from a high resolution scan we used the free software ImageJ (https://imagej.nih.gov/ij/index.html; [68]. We extracted a record of grey intensity values ranging from black (grey value 0) and white (grey value 255) at a spatial resolution of 20 µm following the procedure given in Breitenbach and Marwan (2023)[67]. The greyscale record follows the growth axis, and for layer counting we developed several lines parallel to the master profile. Using the master grey scale profile, we then counted grey maxima throughout the stalagmite, assuming that couplets of darker and brighter laminae represent one year of deposition. In stalagmite CCB-1 we counted 104 years back from 2019, the year of collection.

Age modelling

The age model for CCB-1 was constructed using the COPRA software[36]. Using 2,000 Monte Carlo simulations for the $\delta^{18}O$ and $\delta^{13}C$ records, COPRA calculates median ages and 95% confidence intervals. For the age model we used the layer counting results and the U-Th dates as absolute ages. The year of collection and inscription in the chamber were used as maximum and minimum ages.

Stable isotope analysis

Six hundred powder samples were collected for stable isotope analysis by continuously milling at 50 µm resolution using a high precision micromill (Sherline 5400 Deluxe) at the Université de Rouen Normandy. Samples were analysed for $\delta^{18}O$ and $\delta^{13}C$ using a ThermoFisher Scientific Delta V Advantage isotope ratio mass spectrometer (IRMS) coupled with a ConFlo IV and a Gasbench II at the Department of Geography and Environmental Sciences, Northumbria University, following the methodology of Spötl[69] and Breitenbach and Bernasconi[70]. The raw isotope values were corrected using the in-house carbonate standard Plessen (for sample size and drift; $n = 10$ per run) and the international standards NBS18, NBS19, and IAEA603 (for 'stretching' correction; $n = > 3$ per standard, per run). In-house standard Pol-2 was measured in each run as control for long-term accuracy. Isotope results are reported in delta notation against the international Vienna PeeDee Belemnite (VPDB) standard. The long-term external precision of both $\delta^{18}O$ and $\delta^{13}C$ is 0.1 ‰ (1 standard deviation) or better.

LA-ICPMS analysis

Laser Ablation Inductively Coupled Plasma Mass Spectrometry (LA-ICPMS) was used to quantify the trace element concentrations of the stalagmite along a track parallel to the growth direction. The analyses were conducted at Department of Earth Sciences, Durham University, using a 193 nm ArF Teledyne Analyte Excite + excimer laser system coupled with a ThermoFisher iCAP TQ ICP-MS. The laser ablated material within a 10×140 µm rectangular spot, with the spot's long dimension oriented perpendicular to the growth axis, parallel to growth horizons[71]. Concentration data were obtained for 11 elements (Mg, Al, Si, P, Ca, Cu, Sr, Ba, Pb, Th, and U) along the entire growth axis of CCB-1 at a sample advance rate of 10 µm s^{-1} and a 15 Hz laser repetition rate. NIST 610 and 612 glasses were used as external standards to quantify any instrumental drift and to derive elemental concentrations. The sample was cleaned thoroughly prior to analysis, and a pre-ablation track run to remove any remaining impurities. A secondary parallel track was run to replicate the results of the main track. Dynamic time warping (DTW) techniques were used within Matlab to wiggle match the trace element to the $\delta^{13}C$ data, thereby correcting for lateral offsets in the stalagmite laminae. The DTW reduced the resolution of the trace element data but ensures its temporal consistency with the $\delta^{13}C$ dataset.

Modelled data for drought index

The few available local instrumental data of the study area (see supplementary methods), drove us to search for modelled climate data and we chose to work with the standardized precipitation evapotranspiration index (SPEI). This index was used for drought analysis and measures the normalised differences of the climatic water balance, by subtracting potential evapotranspiration of precipitation (P-PET)[72]. The PET is part of the CRU (Climatic Research Unit) v4 dataset[73] and is computed with the Penman–Monteith Eq. [74]. PET values were extracted from this dataset using the coordinates of Caumont cave. Values were normalised to log-logistic probability distributions[26] using the R package SPEI (https://cran.r-project.org/web/packages/SPEI/index.html). The obtained SPEI record covers the period 1902 – 2021, with a spatial resolution of 0.5°×0.5°. SPEI numbers are given per monthly values (January to December) with different accumulation periods (3, 6, 9, and 12 months). For this study we used the accumulation period of 6 months until October (dry period). SPEI data is given in positive values, corresponding to positive infiltration, and negative values for dry conditions (water loss to evapotranspiration). Here we focused on October SPEI6 negative values, classified as: i) moderate drought (-1 to -1.5), ii) severe drought (-1.5 and -2), and iii) extreme drought (< -2)[60]. The combined dataset Rouen-Boos and PET extracted from CRU V4 were used to estimate effective infiltration.

Data availability

The datasets generated and/or analysed during the current study are available in the Zenodo repository, with the link: https://doi.org/10.5281/zenodo.13912742.

Received: 21 August 2024; Accepted: 24 October 2024
Published online: 30 October 2024

References

1. Vicente-Serrano, S. M. et al. Long-term variability and trends in meteorological droughts in Western Europe (1851–2018). *Int. J. Climatol.* **41**, E690–E717 (2021).
2. Vidal, J.-P. et al. Multilevel and multiscale drought reanalysis over France with the Safran-Isba-Modcou hydrometeorological suite. *Hydrol. Earth Syst. Sci.* **14**, 459–478 (2010).
3. World Meteorological Organization (WMO). *WMO Atlas of Mortality and Economic Losses from Weather, Climate and Water Extremes (1970–2019)*. 90 https://library.wmo.int/records/item/57564-wmo-atlas-of-mortality-and-economic-losses-from-weather-climate-and-water-extremes-1970-2019 (2021).
4. Smith, A. B. & Matthews, J. L. Quantifying uncertainty and variable sensitivity within the US billion-dollar weather and climate disaster cost estimates. *Nat Hazards* **77**, 1829–1851 (2015).
5. Bakke, S., Ionita, M. & Tallaksen, L. M. The 2018 northern European hydrological drought and its drivers in a historical perspective. Hydrology and Earth System Sciences https://doi.org/10.5194/hess-2020-239 (2020).
6. Dai, A., Zhao, T. & Chen, J. Climate change and drought: A precipitation and evaporation perspective. *Curr Clim Change Rep* **4**, 301–312 (2018).
7. Van Loon, A. F. et al. Drought in a human-modified world: reframing drought definitions, understanding, and analysis approaches. *Hydrology and Earth System Sciences* **20**, 3631–3650 (2016).
8. Wilhite, D. A. & Glantz, M. H. Understanding: The drought phenomenon: the role of definitions. *Water International* https://doi.org/10.1080/02508068508686328 (1985).
9. Büntgen, U. et al. Recent European drought extremes beyond Common Era background variability. *Nat. Geosci.* **14**, 190–196 (2021).
10. Labuhn, I. Climate Variability in Southwest France During the Last 2000 Years : Proxy Calibration and Reconstruction of Drought Periods Based on Stable Isotope Records from Speleothems and Tree Rings. (2014).
11. Büntgen, U. et al. Filling the Eastern European gap in millennium-long temperature reconstructions. *Proceedings of the National Academy of Sciences* **110**, 1773–1778 (2013).
12. Nagavciuc, V. et al. Defining a precipitation stable isotope framework in the wider Carpathian Region. *Water* **14**, 2547 (2022).
13. GIEC. *Publication du 6e rapport de synthèse du GIEC*. https://www.ecologie.gouv.fr/publication-du-6e-rapport-synthese-du-giec (2023).
14. Valo, M. Droughts threaten most of France this summer. *Le Monde.fr* (2022).
15. Woods, M. Drought provokes shutdown of nuclear reactors in northeast France. *RFI* (2020).
16. Camenisch, C. & Salvisberg, M. Droughts in Bern and Rouen from the 14th to the beginning of the 18th century derived from documentary evidence. *Climate of the Past* **16**, 2173–2182 (2020).
17. Cook, B. I. et al. Megadroughts in the common era and the anthropocene. *Nat Rev Earth Environ* **3**, 741–757 (2022).
18. Cheng, H., Sinha, A., Wang, X., Cruz, F. W. & Edwards, R. L. The Global Paleomonsoon as seen through speleothem records from Asia and the Americas. *Clim Dyn* **39**, 1045–1062 (2012).
19. Fairchild, I. J. & Baker, A. *Speleothem Science: From Process to Past Environments* (Wiley, 2012).
20. Genty, D. et al. Precise dating of Dansgaard-Oeschger climate oscillations in western Europe from stalagmite data. *Nature* **421**, 833–837 (2003).
21. Carolin, S. A. *et al.* Precise timing of abrupt increase in dust activity in the Middle East coincident with 4.2 ka social change. *Proceedings of the National Academy of Sciences* **116**, 67–72 (2019).
22. Nicholson, S. L., Jacobson, M. J., Hosfield, R. & Fleitmann, D. The Stalagmite Record of Southern Arabia: Climatic Extremes, Human Evolution and Societal Development. *Front. Earth Sci.* **9** (2021).
23. Fairchild, I. J. et al. Controls on trace element (Sr–Mg) compositions of carbonate cave waters: Implications for speleothem climatic records. *Chemical Geology* **166**, 255–269 (2000).
24. Sinclair, D. J. Two mathematical models of Mg and Sr partitioning into solution during incongruent calcite dissolution: Implications for dripwater and speleothem studies. *Chemical Geology* **283**, 119–133 (2011).
25. Wassenburg, J. A. et al. Calcite Mg and Sr partition coefficients in cave environments: Implications for interpreting prior calcite precipitation in speleothems. *Geochimica et Cosmochimica Acta* **269**, 581–596 (2020).
26. Vicente-Serrano, S. M., Beguería, S. & López-Moreno, J. I. A Multiscalar drought index sensitive to global warming: The standardized precipitation evapotranspiration index. *Journal of Climate* **23**, 1696–1718 (2010).
27. Nehme, C. et al. Reconstructing fluvial incision rates based on palaeo-water tables in chalk karst networks along the Seine valley (Normandy, France). *Earth Surface Processes and Landforms* **45**, 1860–1876 (2020).
28. Bejarano-Arias, I. et al. Climate monitoring in the Caumont cave and quarry system (northern France) reveal near oxygen isotopic equilibrium conditions for carbonate deposition. *IJS* **53**, 13–23 (2024).

29. Ballesteros, D. et al. Going with the flow: Sedimentary processes along karst conduits within Chalk aquifers, northern France. *Sedimentary Geology* **452**, 106422 (2023).
30. Chevalier, S. Apport de la cartographie 2D et 3D dans l'appréhension des aléas géomorphologues du sous-sol : cas d'étude des carrières-grottes de Caumont (Normandie). (Université de Rouen Normandie, 2022).
31. Fronteau, G., Moreau, C., Thomachot-Schneider, C. & Barbin, V. Variability of some Lutetian building stones from the Paris Basin, from characterisation to conservation. *Engineering Geology* **115**, 158–166 (2010).
32. Ballesteros, D. et al. Stratigraphical influence on chalk cave development in Upper Normandy, France: Implications for chalk hydrogeology. *International Journal of Speleology* **49**, 187–208 (2020).
33. Cantat, O. Analyse critique sur les tendances pluviométriques au 20ème siècle en Basse-Normandie : réflexions sur la fiabilité des données et le changement climatique. *Annales de l'Association Internationale de Climatologie* **1**, 11–31 (2004).
34. Diomard, I. & Chéron, E. *Etat Des Lieux Sur Le Changement Climatique et Ses Incidences Agricoles En Région Normandie*. 152 (2020).
35. Roy-Barman, M. & Pons-Branchu, E. Improved U-Th dating of carbonates with high initial 230Th using stratigraphical and coevality constraints. *Quaternary Geochronology* **32**, 29–39 (2016).
36. Breitenbach, S. F. M. et al. Constructing proxy records from age models (COPRA). *Climate of the Past* **8**, 1765–1779 (2012).
37. Baldini, J. U. L. et al. Biomass effects on stalagmite growth and isotope ratios: A 20th century analogue from Wiltshire, England. *Earth and Planetary Science Letters* **240**, 486–494 (2005).
38. Fairchild, I. J. & Treble, P. C. Trace elements in speleothems as recorders of environmental change. *Quaternary Science Reviews* **28**, 449–468 (2009).
39. Ionita, M. et al. The European 2015 drought from a climatological perspective. *Hydrology and Earth System Sciences* **21**, 1397–1419 (2017).
40. Lestienne, C. La sécheresse de 1921, calamité historique. *LEFIGARO* (2023).
41. Mazuir, V. & Bibily, C. Retour sur les sécheresses en France depuis 1976. *Les Echos* (2022).
42. Séchet, G. Les chroniques météo de l'année 1934. *Meteo-Paris* https://www.meteo-paris.com/chronique/annee/1934 (2003).
43. Trzpit, J.-P. sécheresse en Basse-Normandie : calamité accidentelle ou mal récurrent ?. *Études Normandes* **27**, 55–74 (1978).
44. van der Schrier, G. et al. The 1921 European drought: impacts, reconstruction and drivers. *Climate of the Past* **17**, 2201–2221 (2021).
45. Barker, L. J. et al. Historic hydrological droughts 1891–2015: Systematic characterisation for a diverse set of catchments across the UK. *Hydrology and Earth System Sciences* **23**, 4583–4602 (2019).
46. Hänsel, S., Hoy, A., Brendel, C. & Maugeri, M. Record summers in Europe: Variations in drought and heavy precipitation during 1901–2018. *International Journal of Climatology* **42**, 6235–6257 (2022).
47. Ionita, M., Dima, M., Nagavciuc, V., Scholz, P. & Lohmann, G. Past megadroughts in central Europe were longer, more severe and less warm than modern droughts. *Commun Earth Environ* **2**, 1–9 (2021).
48. Markonis, Y. *et al.* The rise of compound warm-season droughts in Europe. *Science Advances* **7**, eabb9668 (2021).
49. Hanel, M. et al. Revisiting the recent European droughts from a long-term perspective. *Sci Rep* **8**, 9499 (2018).
50. Spinoni, J., Naumann, G. & Vogt, J. V. Pan-European seasonal trends and recent changes of drought frequency and severity. *Global and Planetary Change* **148**, 113–130 (2017).
51. Flipo, N. *et al.* Pluri-annual Water Budget on the Seine Basin: Past, Current and Future Trends. in *The Seine River Basin* (eds. Flipo, N., Labadie, P. & Lestel, L.) 59–89 (Springer International Publishing, Cham, 2021). https://doi.org/10.1007/698_2019_392.
52. van der Velde, M., Tubiello, F. N., Vrieling, A. & Bouraoui, F. Impacts of extreme weather on wheat and maize in France: evaluating regional crop simulations against observed data. *Climatic Change* **113**, 751–765 (2012).
53. Braun, T. et al. Decline in seasonal predictability potentially destabilized Classic Maya societies. *Commun Earth Environ* **4**, 1–12 (2023).
54. Fohlmeister, J. et al. Main controls on the stable carbon isotope composition of speleothems. *Geochimica et Cosmochimica Acta* **279**, 67–87 (2020).
55. Genty, D. *et al.* Dead carbon in stalagmites: carbonate bedrock paleodissolution vs. ageing of soil organic matter. Implications for 13C variations in speleothems. *Geochimica et Cosmochimica Acta* **65**, 3443–3457 (2001).
56. Allan, M. et al. Evidence for solar influence in a Holocene speleothem record (Père Noël cave, SE Belgium). *Quaternary Science Reviews* **192**, 249–262 (2018).
57. Baldini, J. U. L. et al. Detecting and quantifying palaeoseasonality in stalagmites using geochemical and modelling approaches. *Quaternary Science Reviews* **254**, 106784 (2021).
58. Sinclair, D. J. et al. Magnesium and strontium systematics in tropical speleothems from the Western Pacific. *Chemical Geology* **294–295**, 1–17 (2012).
59. Kingston, D. G., Stagge, J. H., Tallaksen, L. M. & Hannah, D. M. European-scale drought: Understanding connections between atmospheric circulation and meteorological drought indices. *Journal of Climate*. https://doi.org/10.1175/JCLI-D-14-00001.1 (2015).
60. Ionita, M. & Nagavciuc, V. Changes in drought features at the European level over the last 120 years. *Nat. Hazards Earth Syst. Sci.* **21**, 1685–1701 (2021).
61. Ionita, M., Boroneant, C. & Chelcea, S. M. Seasonal modes of dryness and wetness variability over Europe and their connections with large scale atmospheric circulation and global sea surface temperature. *Climate Dynamics* (2015).
62. Bakke, S. J., Ionita, M. & Tallaksen, L. M. Recent European drying and its link to prevailing large-scale atmospheric patterns. *Sci Rep* **13**, 21921 (2023).
63. Pons-Branchu, E. et al. A geochemical perspective on Parisian urban history based on U-Th dating, laminae counting and yttrium and REE concentrations of recent carbonates in underground aqueducts. *Quaternary Geochronology* **24**, 44–53 (2014).
64. Pons-Branchu, E. *et al.* U-series and radiocarbon cross dating of speleothems from Nerja Cave (Spain): Evidence of open system behavior. Implication for the Spanish rock art chronology. *Quaternary Science Reviews* **290**, 107634 (2022).
65. Cheng, H. et al. Improvements in 230Th dating, 230Th and 234U half-life values, and U-Th isotopic measurements by multi-collector inductively coupled plasma mass spectrometry. *Earth and Planetary Science Letters* **371–372**, 82–91 (2013).
66. Jaffey, A. H., Flynn, K. F., Glendenin, L. E., Bentley, W. C. & Essling, A. M. Precision measurement of half-lives and specific activities of 235U and 238U. *Phys. Rev. C* **4**, 1889–1906 (1971).
67. Breitenbach, S. F. M. & Marwan, N. Acquisition and analysis of greyscale data from stalagmites using ImageJ software. *Cave and Karst Science* **50**, 69–78 (2023).
68. Schneider, C. A., Rasband, W. S. & Eliceiri, K. W. NIH image to ImageJ: 25 years of Image Analysis. *Nat Methods* **9**, 671–675 (2012).
69. Spötl, C. A simple method of soil gas stable carbon isotope analysis. *Rapid Communications in Mass Spectrometry* **18**, 1239–1242 (2004).
70. Breitenbach, S. F. M. & Bernasconi, S. M. Carbon and oxygen isotope analysis of small carbonate samples (20 to 100 µg) with a GasBench II preparation device. *Rapid Communications in Mass Spectrometry* **25**, 1910–1914 (2011).
71. Müller, W., Shelley, M., Miller, P. & Broude, S. Initial performance metrics of a new custom-designed ArF excimer LA-ICPMS system coupled to a two-volume laser-ablation cell. *J. Anal. At. Spectrom.* **24**, 209–214 (2009).
72. Bakke, S., Ionita, M. & Tallaksen, L. M. Recent European drying and its link to prevailing large-scale atmospheric patterns. *Scientific Reports* https://doi.org/10.21203/rs.3.rs-2397739/v1 (2022).

73. Harris, I., Osborn, T. J., Jones, P. & Lister, D. Version 4 of the CRU TS monthly high-resolution gridded multivariate climate dataset. *Sci Data* **7**, 109 (2020).
74. Vanderlinden, K., Giráldez, J. V. & Meirvenne, M. V. Spatial Estimation of Reference Evapotranspiration in Andalusia, Spain. *Journal of Hydrometeorology* **9**, 242–255 (2008).

Acknowledgements
We would like to thank the Region Normandy for funding the PhD project and RIN- PALECONOR (2019-2022) project that funded the analysis and fieldwork. Similarly, to the laboratory team at the department of Geography and Environmental Sciences, Northumbria University, Newcastle, United Kingdom for stable isotope analysis and for providing the facilities for the preparation and measurements. We are grateful to the Panoply technical platform for the U/Th measurements, to A. Dapoigny for assistance during MC-ICPMS measurement and the Department of Earth Sciences, Durham University, UK for the trace elements analysis. Lastly, we thank the French Federation of speleology and canyoning for providing access to the Caumont quarry and cave system.

Author contributions
CN and DM designed and directed the study. IB did the fieldwork under the supervision of CN, and wrote the manuscript (original version). The sampling of the stalagmites was done by IB under the guidance of CN. The measurements and analysis of modern carbonate was done by IB with the supervision and assistance of SB, SM and SU. U/Th dating were done by EP-B and the trace element measurements by JB. The modelled climatic data (SPEI) for the study area was provided by MI as well as the guidance for their interpretation. All authors contributed to discussion of the results and to the review of the manuscript.

Declarations

Competing interests
The authors declare no competing interests.

Additional information
Supplementary Information The online version contains supplementary material available at https://doi.org/10.1038/s41598-024-77674-2.

Correspondence and requests for materials should be addressed to I.B.-A.

Reprints and permissions information is available at www.nature.com/reprints.

Publisher's note Springer Nature remains neutral with regard to jurisdictional claims in published maps and institutional affiliations.